MAGMA (2004) 17: 249–259
DOI 10.1007/s10334-004-0079-z

REVIEW ARTICLE

Diffusion imaging for evaluation of tumor therapies in preclinical animal models

B. A. Moffat
D. E. Hall
J. Stojanovska
P. J. McConville
J. B. Moody
T. L. Chenevert
A. Rehemtulla
B. D. Ross

Received: 29 June 2004
Revised: 22 September 2004
Accepted: 7 October 2004
Published online: 1 December 2004

B. A. Moffat (✉) · D. E. Hall
J. Stojanovska · T. L. Chenevert · B. D. Ross
Center for Molecular Imaging,
Department of Radiology,
University of Michigan,
Ann Arbor,
1150 W. Medical Center Drive,
MSRB III Rm 9303,
Ann Arbor, MI
48109-0503, USA
E-mail: bmoffat@umich.edu
Tel.: +1-734-6158645
Fax: +1-734-6472563

A. Rehemtulla
Department of Radiation Oncology,
University of Michigan,
Ann Arbor,
1150 W. Medical Center Drive,
MSRB III Rm 9303,
Ann Arbor, MI
48109-0503, USA

P. J. McConville · J. B. Moody
Molecular Imaging Research, 924 N. Main,
Ann Arbor,
MI 48104, USA
www.molecularimaging.com

Abstract The increasing development of novel targeted therapies for treating solid tumors has necessitated the development of technology to determine their efficacy in preclinical animal models. One such technology that can non-invasively quantify early changes in tumor cellularity as a result of an efficacious therapy is diffusion MRI. In this overview we present some theories as to the origin of diffusion changes as a result of tumor therapy, a robust methodology for acquisition of apparent diffusion coefficient maps and some applications of determining therapeutic efficacy in a variety therapeutic regimens and animal models.

Keywords Apparent diffusion coefficient · ADC · Diffusion · Tumor · Therapeutic efficacy · MRI · NMR

Introduction

Rodent cancer models have become indispensable in the discovery and assessment of new anticancer agents [1]. Lead compounds that are identified as having anti-tumor activity using in vitro screening assays are subsequently evaluated in vivo using rodent models [2, 3]. Rapidly growing transplantable mouse or human tumor cell lines grown subcutaneously or orthotopically in syngeneic or immuno-deficient rodents allow for quantification of tumor growth and treatment response monitoring using caliper, colony-forming efficient assays [4–6] or anatomical imaging (such as T_2-weighted MRI) measurements of tumor volume [7].

These traditional methods provide effective ways in which to quantify cancer therapeutic efficacy. However, non-invasive surrogate markers of therapeutic efficacy in

animal models are needed for several reasons. Firstly, there are no clinical equivalent measurements that can be performed during phase II and III trials to relate clinical efficacy back to those observed in preclinical models. Biopsies are usually acquired pre-treatment but are rarely (if at all) acquired during or after therapy. In addition, traditional radiological response (reduction in tumor volume) is typically only acquired once, several months after therapy. This response is a complex result of not only therapeutic efficacy but also patient and tumor characteristics such as patient age and tumor stage. Therefore it is almost impossible to relate these clinical outcomes to anything measured in preclinical animal testing. Secondly, these radiological and colony-forming assays have no way of quantifying regional heterogeneity in tumor response. Spatial differences in tumor treatment response can be a confounding problem in clinical and experimental therapeutics. These can arise from regional differences in perfusion, chemosensitivity and also nonuniform drug delivery (e.g. delivery/expression of transgene during gene therapy). Thirdly, earlier and more sensitive/predictive methods to determine treatment efficacy during the initial course of treatment would be extremely valuable for facilitating therapeutic protocol planning. Since many therapeutic agents such as chemotherapy are frequently given in fractionated cycles, an early assessment of therapeutic response during the initial phase of administration would provide an opportunity to gauge optimum dosage and also provide feedback related to the optimum dose frequency.

Development of early indicators of treatment response which could also provide information related to the spatial heterogeneity of the effects of treatment would be of significant benefit for both experimental and clinical trials. These issues underscore the need for using noninvasive imaging to facilitate the evaluation of the responsiveness of experimental tumors in preclinical therapeutic studies. In this regard, largely untapped potential resides in MRI methods known to be sensitive to tissue structure at the cellular level. Such information may be derived via measurement of tissue properties that reflect dynamics in the microscopic environment.

Since molecular and cellular changes precede macroscopic changes in tumor size, it would be ideal to have an assay that could quantify these changes both in clinical cancer therapeutics and preclinical drug trials. For the last ten years diffusion MRI has been under active investigation as a possible surrogate marker of anti-tumor therapeutic efficacy [8–19]. As depicted in Fig. 1, treatment of tumors may result in damage and/or killing of cells, thus altering the integrity of cell membranes and thereby increasing the fractional volume of the interstitial space due to apoptotic body formation and cell loss. These changes have been shown to increase the diffusion of water in the damaged tumor tissue [14,15,17]. Diffusion of water within tissue can be non-invasively

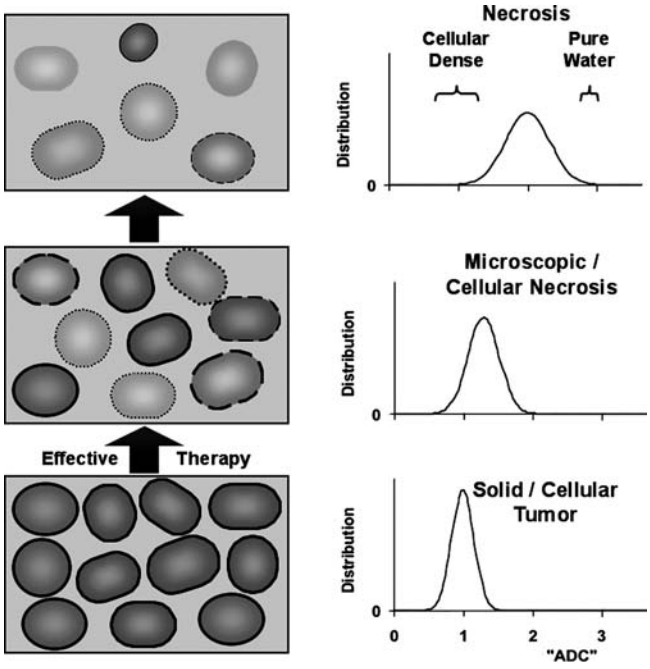

Fig. 1 Schematic representation of the relationship between change in tissue cellularity and molecular water mobility measured as an "apparent diffusion coefficient" (ADC). On the left is the evolution toward necrosis following an effective therapy. The increases in extracellular space and membrane permeability allow greater water mobility, as illustrated by distributions of diffusion on the right. (Used with permission from Ross et al. [10])

quantified as an apparent diffusion coefficient (ADC) by using diffusion MRI. The diffusion of water within the tumor is often heterogeneous, particularly during therapy, therefore water diffusion within the tumor is often represented by an ADC histogram, as shown in Fig. 1. ADC is negatively correlated with tumor cell density, as shown in Fig. 2; therefore shifts in these ADC histograms to higher ADC values can be an early and quantifiable indicator of therapeutic efficacy. One additional advantage of measuring ADC is that it is independent of magnetic field strength and is a biophysical property of the tissue itself therefore making it much more comparable from scanner to scanner than most other MR properties.

Initial studies using diffusion MRI to detect changes in water diffusion in animal tumor models following high-dose chemotherapy were found to be very promising [8, 15,19]. Changes in ADC values were observed to precede changes in tumor growth kinetics and tumor regression, indicating the potential for applying this approach to early predictive monitoring of cancer therapy. In addition there have now been several clinical studies that have shown correlations between early increases in ADC and tumor response to therapy [10,14,20–22].

There is tremendous potential for diffusion MRI to become an important surrogate biomarker for cancer

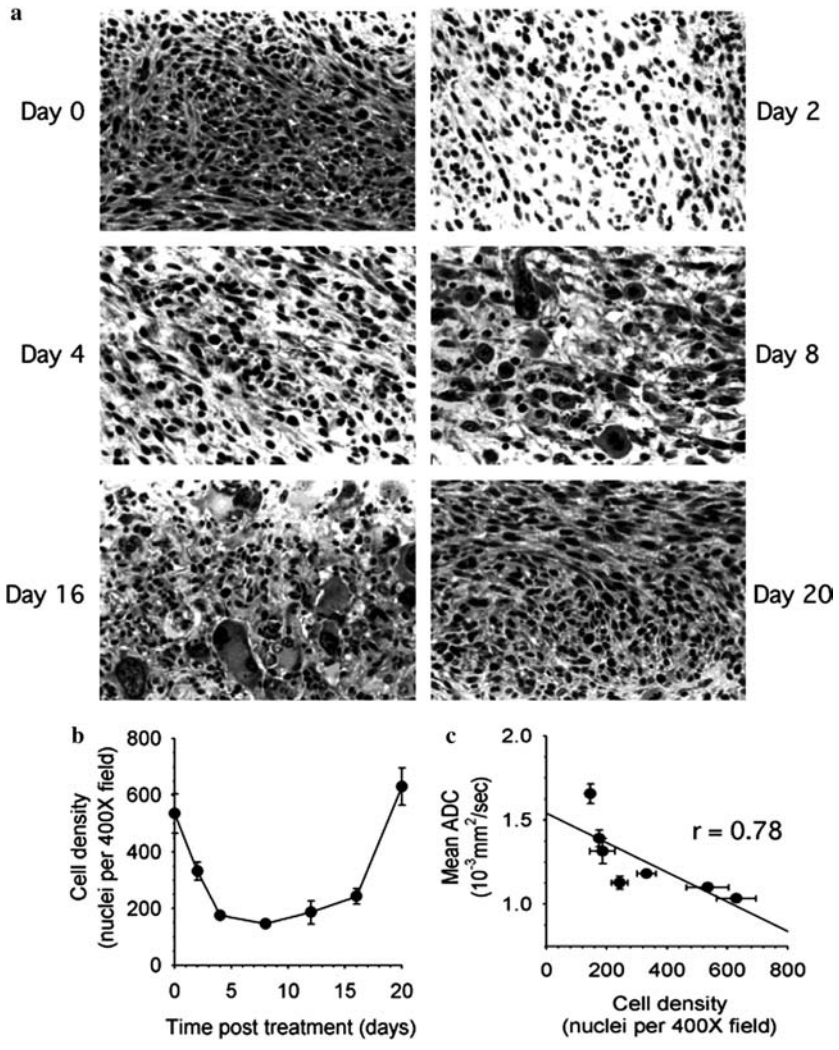

Fig. 2 H and E stained histology slides (**a**) showing decreasing cellularity 9L tumors following treatment with a 13.3 mg/kg dose of BCNU (**b**). Changes in mean tumor ADC correlated with these histological changes (**c**). (Used with permission of Chenevert et al. [14])

therapeutic efficacy. Further clinical and preclinical studies are underway to evaluate the universality of ADC response to therapeutic efficacy. ADC imaging of animal tumor models with standard therapies can help further to refine and validate ADC imaging as a surrogate marker. In addition imaging of experimental therapeutic regimens will also aid in extending its utility into these new 'molecularly targeted' therapeutic approaches.

In this paper, an overview of the use of diffusion MRI as a surrogate marker for evaluating cancer therapeutic efficacy in animal models is presented. This will provide some examples and strategies of quantifying ADC changes and evaluating how these relate to cancer therapeutic efficacy.

The diffusion pulse sequence

Perhaps the single greatest challenge in the implementation of diffusion imaging is to acquire quantitative diffusion-weighted images in the presence of physiological motion that are free from artifacts. While diffusion echo planar imaging (EPI) has revolutionized clinical diffusion MRI, diffusion MRI of animal models remains problematic. EPI on higher field (7 T and above) animal MRI scanners can be complicated due to issues such as shortened tissue transverse relaxation and the requirement for higher resolution. For this reason conventional, spin-echo-based methods are usually preferred.

In order to achieve artifact-free longitudinal diffusion imaging of rodent cancer models in a high-throughput environment, a practical yet robust diffusion pulse sequence and protocol is needed. This strategy must be able to acquire high-resolution multi-slice diffusion data within a reasonable time frame (10–20 min), with minimal animal preparation and with minimal motion artifacts. Presented

here is a practical diffusion pulse sequence (Fig. 3) and protocol that has been designed for routine 'high-throughput' imaging of animal models. The pulse sequence and reconstruction methodology combines the previously developed concepts of spin echo multi-slice imaging, isotropic diffusion weighting [23,24], first moment motion and flow compensation [25], and navigator echo correction [26] to produce, high signal-to-noise and high-resolution apparent diffusion coefficient images while requiring only minimal animal preparation and shimming; it is also insensitive to bulk translational and rotational motion due to the animal respiratory cycle.

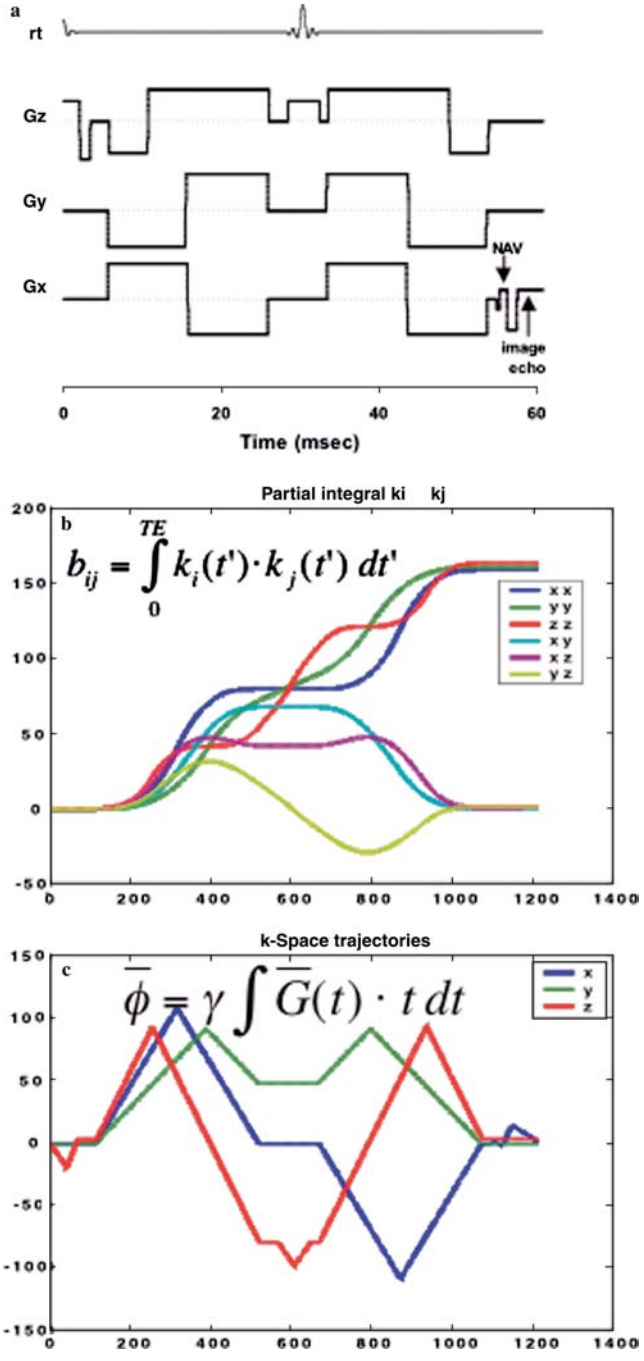

Fig. 3 **a** Gradient waveform for isotropic diffusion weighting, flow compensation and navigator echo. G_x is the read gradient direction, G_y is the phase-encoding direction and G_z is the slice direction. Diffusion gradients on all three gradient directions contribute to the overall "b value". **b** Plot of b values as a function of time during diffusion pulse sequence. **c** Plot of k-space "first moments" as a function of time during the diffusion pulse sequence

Monitoring the diffusion of water using MRI can be accomplished by making the MR signal intensity dependent on water mobility by the application of additional pulsed magnetic field gradients incorporated within the normal MRI sequence [27]. Individual nuclear spins of the tumor water molecules accumulate a phase shift in proportion to their spatial position in these additional gradient fields. After waiting a given evolution time for spins to diffuse, a second gradient pulse is applied to completely refocus or re-phase stationary spins. However water molecules that have diffused during this evolution time do not experience the same magnitude of phase shift and are therefore refocused incompletely. Thus, the paired gradient pulses attenuate signal in proportion to local tissue water mobility according to the Stejskal–Tanner equation [28]:

$$\ln\left[\frac{S}{S_0}\right] = -b \times \mathrm{ADC}; \tag{1}$$

where

$$b = \delta\left(\Delta - \frac{\delta}{3}\right)\gamma^2 G^2 \tag{2}$$

S is the diffusion-weighted signal, S_0 is the intrinsic MR signal, δ is the duration of the diffusion-encoding gradient pulses, Δ is the time between the diffusion gradients, γ is the gyro-magnetic ratio and G is the diffusion-encoding gradient amplitude. Quantitative measurements of diffusion coefficient (ADC) values are obtained by measuring signal attenuation as a function of varying gradient strength and evolution time. In many tissues (including brain) the diffusion of water is anisotropic, i.e., the rate of diffusion is more or less restricted depending on the direction of the diffusion gradients (G) relative to the underlying cellular structure. For measuring changes in the underlying tumor morphology the rotationally invariant mean ADC needs to be measured. This can be achieved in two ways. Firstly and most simply one can measure ADC using three different gradient sensitizations that are orthogonal to each other (e.g. G_x, G_y, G_z), such that ADC can be given by:

$$\mathrm{ADC}_{\mathrm{av}} = \frac{\left(\mathrm{ADC}_x + \mathrm{ADC}_y + \mathrm{ADC}_z\right)}{3}. \tag{3}$$

This has the disadvantage that it requires at least four images to be acquired to calculate $\mathrm{ADC}_{\mathrm{av}}$. While this is unproblematic in clinical echo planar imaging where the images only take seconds to acquire, in animal

imaging studies when spin-echo-based sequences are used the acquisition of two extra images can increase scan times by the order of 20 min.

One way to reduce the scan time is to change the direction of the diffusion sensitization gradients during the diffusion period (Fig. 1) such that the diffusion weighting is equally applied in three orthogonal directions.

In the case of a generalized waveform of diffusion sensitization the following applies:

$$\overline{G}(t) = \begin{bmatrix} G_x(t) & G_y(t) & G_z(t) \end{bmatrix}$$

$$\overline{k}(t) = \gamma \int_0^t \overline{G}(t')\,\mathrm{d}t'$$

$$b = \int_0^{TE} \overline{k}(t')^{\mathrm{T}} \cdot \overline{k}(t')\mathrm{d}t' = \begin{bmatrix} b_{xx} & b_{xy} & b_{xz} \\ b_{yx} & b_{yy} & b_{yz} \\ b_{zx} & b_{zy} & b_{zz} \end{bmatrix} \tag{4}$$

If

$$b_{xx} = b_{yy} = b_{zz} = b_0; \quad \text{and} \quad b_{xy} \approx b_{xz} \approx b_{yz} \approx 0$$

then

$$\ln\left[\frac{S_0}{S}\right] = b_0\{\mathrm{ADC}_{xx} + \mathrm{ADC}_{yy} + \mathrm{ADC}_{zz}\} \tag{5}$$

Equation (5) then, is essentially a rotationally invariant form of the Stjeskal–Tanner equation (1) where the rotationally invariant ADC value is given by Eq. (3). From Eqs. (4) and (5) it is necessary to note that, to achieve isotropic diffusion weighting in a single scan, the waveform of the applied magnetic field gradients must be such that the diagonals of the 'b-matrix' are equal and the off-diagonals are as close to zero as possible [23]. Figure 3b shows the evolution of the elements of the 'b-matrix' during the diffusion pulse sequence shown in Fig. 3a. Note that at the echo center the diagonal elements of the matrix b are essentially equal while the off-diagonals are minimized.

As discussed above motion artifacts present a significant problem in spin echo diffusion imaging sequences. This generally presents itself as large ghosting artifacts in the phase-encoding direction (Fig. 4a). The pulse sequence in Fig. 3a has two methods for reducing these phase-encode artifacts. Firstly, the gradient waveforms were further constrained such that the "first moments" of the gradient waveforms are minimized at the imaging echo center (Fig. 3c). Secondly a 32-point non-phase-encoded echo (navigator echo) is acquired before the imaging echo is acquired. Using this echo it is possible to correct any phase-encode errors during image reconstruction [26] to produce diffusion-weighted images and corresponding ADC maps (Fig. 4b and c) with minimal artifacts.

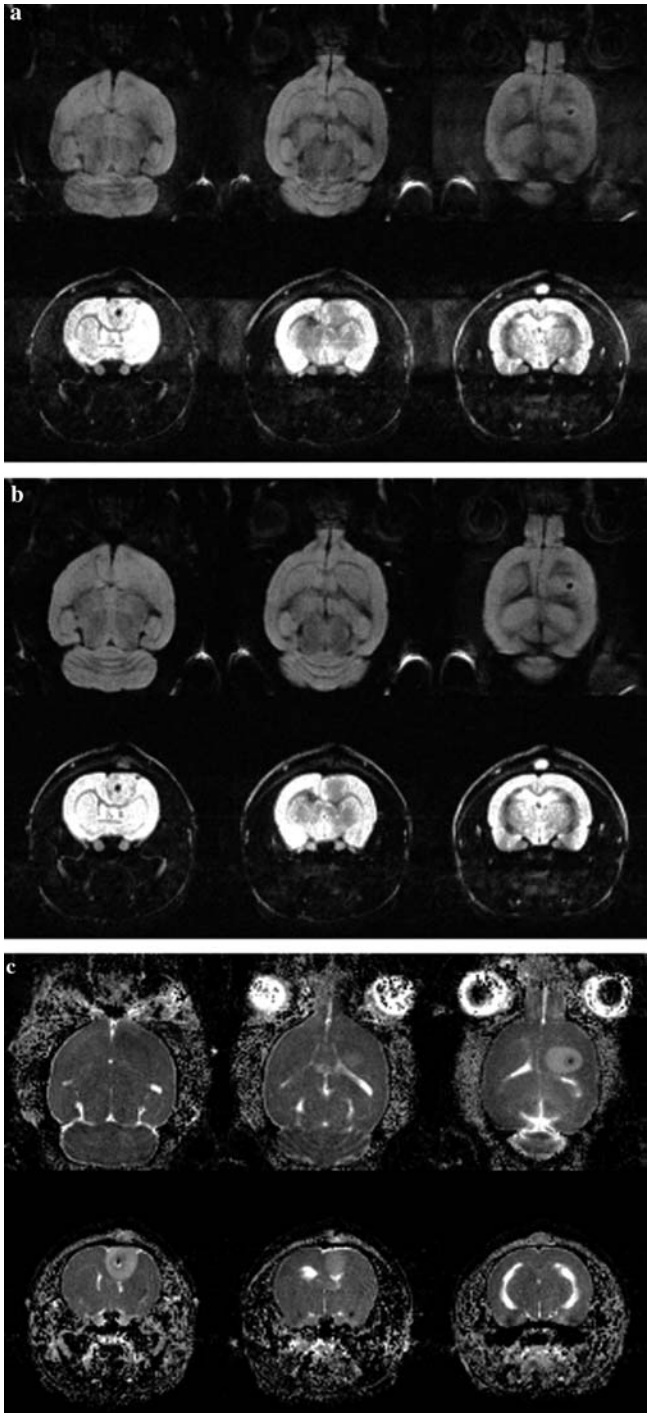

Fig. 4 Diffusion-weighted images without (**a**) and with (**b**) navigator echo correction, and corresponding ADC maps of transverse (*top*) and coronal (*bottom*) through a rat brain

Imaging protocol

In general for the examples presented in this review multiple 1-mm slices were acquired with a 0.5-mm gap and a 3-cm FOV using a standard parallel multi-slice acquisition scheme on a 7-T Varian MRI scanner. The acquisition matrix was 128 × 128 with a 32-point navigator echo that

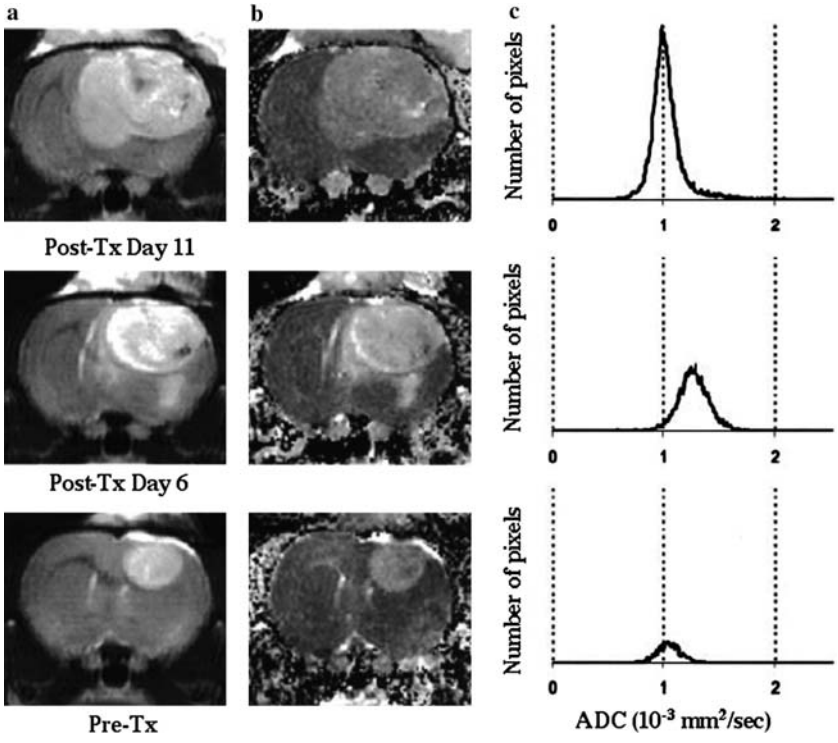

Fig. 5 Illustration of a 9L rat glioma treated with a single "low" dose (6.65 mg/kg) of BCNU chemotherapy. At this low dose, the 9L model mimics the course of a non-responder because tumor growth rate is only slightly retarded. Serial T_2-weighted MR images (**a**) of this animal indicate continued tumor growth. The corresponding ADC maps are illustrated in column (**b**), where brighter pixels represent higher water mobility. The distributions of ADC values within the tumor are illustrated in column (**c**) for these three time points. Note, a slight increase in water diffusion at 6 days after treatment, but the tumor returns to a dense cellular state by day 11. The area under each histogram is proportional to tumor volume. (Used with permission of Ross et al. [10])

was zero filled to 256×256. ADC maps were calculated from two diffusion-weighted data sets with a Δb value of 1148 s/mm^2 and an echo time of 60 ms. Using a recycling time of 3 s, a NEX of two for the "high b value image" and a NEX of one for the "low b value image", the acquisition of the total data set was accomplished in ~17 min. Animals were generally anesthetized using 1.5% isoflurane. During imaging animals were free to breathe normally and were maintained at 37°C using a water pad connected to a heated water recirculation unit.

Chemotherapy dose response of ADC

The usefulness of a surrogate marker for therapeutic efficacy in preclinical animal testing depends on several key attributes. It must be sensitive enough to measure modest therapeutic effects yet it must have a significant dynamic range that it can differentiate between different levels of therapeutic effect. To demonstrate the utility of diffusion MRI for distinguishing a relatively ineffective treatment from an effective treatment, rats with orthotopically implanted gliomas were treated with a single low dose of BCNU (6.65 mg/kg) and a single high dose of BCNU (26.6 mg/kg). Data from the animal treated with the low-dose schedule is shown in Fig. 5. Anatomical T2-weighted images of the brain are shown before and at two time points after treatment along with the corresponding ADC maps and tumor ADC histograms. From the anatomical images, it is clear that the tumor continued to grow, and no regression of the mass was observed. The ADC maps of the brain revealed a slight increase in the tumor signal intensity, which reflects that a small amount of cell killing had occurred [14]. These changes were quantified by segmenting the tumor regions from the ADC maps and plotting a histogram wherein the quantity of pixels (y-axis) were plotted versus the ADC values (x-axis) for the entire tumor mass over time. The area under the histogram curve is proportional to the tumor volume. As shown in the ADC histograms (Fig. 5), there was a slight shift to the right (higher mean diffusion values) at day 6 after treatment, indicating a transient loss of cells from the tumor mass, which recovered by day 11. For preclinical drug studies, the ability of diffusion MRI to detect a small therapeutic effect, especially when the anatomical images were unable to provide any clear evidence of therapeutic benefit, is in fact quite valuable. In this regard, detection of a therapeutic effect in a limited small number of animals could be quantified using diffusion MRI,

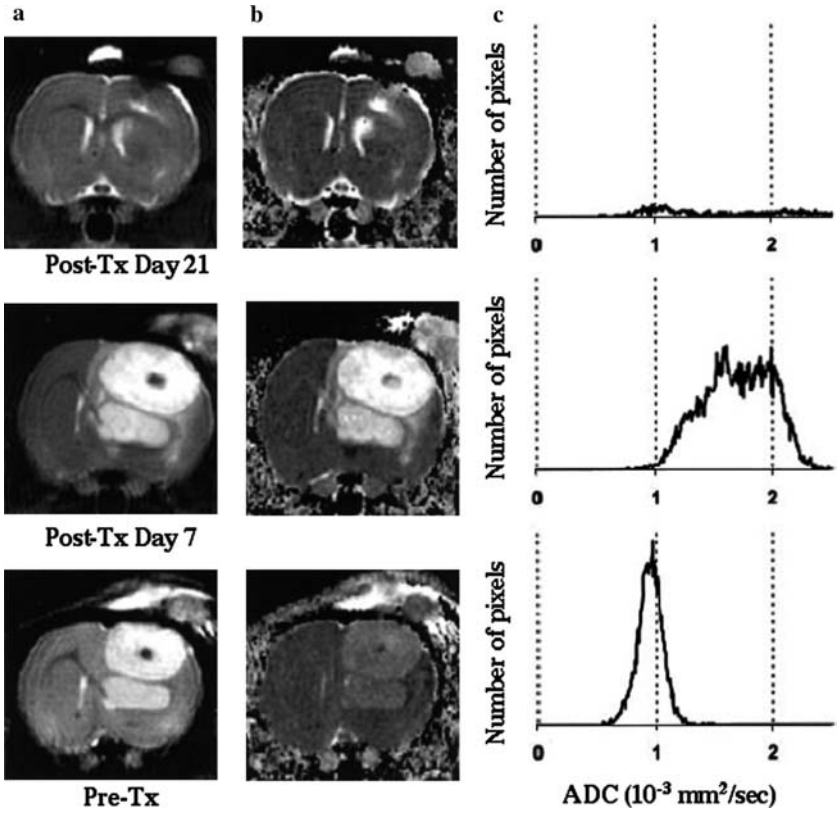

Fig. 6 Illustration of a 9L rat glioma treated with a single "high" dose (26.6 mg/kg) of BCNU chemotherapy. At this high dose, this rat mimics a responder because tumor shrinks substantially. Serial T2-weighted MR images of this animal, shown in column (**a**), illustrate the degree of maximal tumor shrinkage on day 21. The corresponding ADC maps are shown in column (**b**). Despite continued tumor growth on day 7, the increase water mobility is visually apparent on the ADC maps, which suggests necrosis. This is also illustrated graphically in the diffusion histograms (**c**). (Used with permission of Ross et al. [10])

and the decision could be made to increase the dosage to determine whether the drug treatment could be improved. In this brain tumor model system, the dosage of BCNU was increased fourfold, and the results from the anatomical images, ADC maps, and tumor diffusion histograms are shown in Fig. 6. This therapeutic dosage of BCNU resulted in a significant regression of the tumor mass, as observed on day 21 after treatment. A large increase in tumor diffusion values was observed at day 7 as evidenced by the bright tumor signal intensity in the ADC maps as compared with the pretreatment image. It is also important to note that the change in tumor diffusion values preceded regression, indicating that diffusion MRI can detect early therapeutic-induced changes to the tumor. Comparison of the histogram changes of the tumor treated with the high BCNU dose (Fig. 6) with the animal treated with the low dose (Fig. 5) revealed that the magnitude of the diffusion increase varied with therapeutic outcome. Although Figs. 5 and 6 demonstrate isolated examples, the results are quite reproducible in larger cohorts of animals [14]. Results published previously [14] demonstrate that the low dose achieves relatively little to no therapeutic efficacy (0.2 log cell kill) and only modest but significant increase in ADC (~10%) 4 days after chemotherapy. In contrast the high-dose schedule had on average a much larger and significant increase in ADC (~30%) that correlated with a much larger cell kill (~2.0 [7]).

ADC imaging of subcutaneous tumor models

Another example that demonstrates the robustness of the use of diffusion MRI is provided from a study of a subcutaneous PC-3 (prostate) tumor grown in a nude mouse which was treated with 100 mg/kg (i.p.) Camptosar. As shown in Fig. 7, the diffusion increased significantly following treatment, which also corresponded to a dramatic reduction (loss) of tumor growth versus the untreated (control) animal. Although the efficacy of Camptosar in treating PC-3 tumors can be assessed by the volume response, this is not the case when using orthotopic models or in clinical practice. The early diffusion response shows that ADC imaging has the potential to serve as an early surrogate marker of Camptosar therapeutic efficacy both in orthotopic models and in the clinical management of prostate cancer.

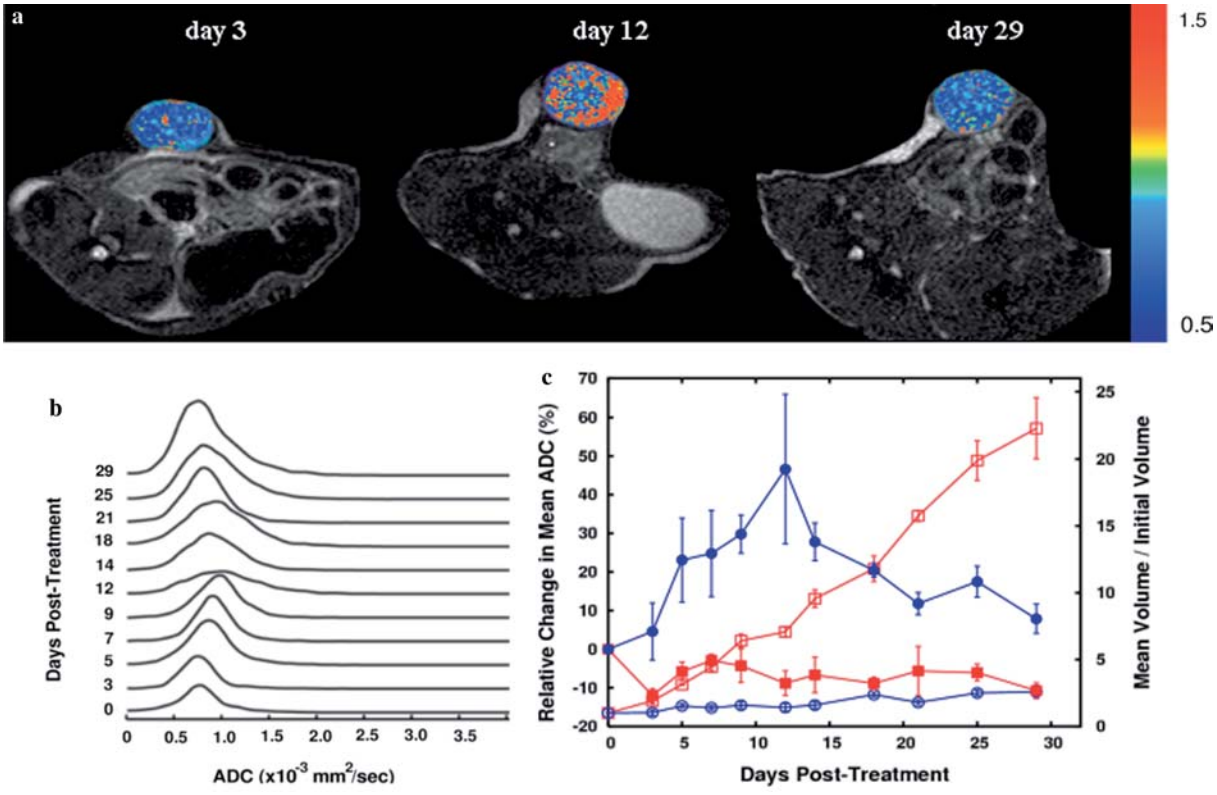

Fig. 7 Diffusion-weighted MRI study of a subcutaneous PC-3 (prostate) tumor in a nude mouse treated with 100 mg/kg (i.p.) Camptosar (unpublished data). **a** The three-grayscale anatomical T2-weighted images are overlaid with a diffusion map (*color*) of the tumor, from left to right (day 3, day 12 and day 29 post-treatment). Note the increase in tumor diffusion values (*blue*) on day 12 post-treatment. Tumor data is also displayed in histogram format over time (**b**) from the same animal as the images. The plot of "Mean relative ADC change (%)" versus time is the change in Mean ADC relative to day 0 of three treated and three control animals **c**. *Solid symbols* are ADC (*circle*=treated, *square*=control) and *open symbols* are volume (*circle*=treated, *square*=control)

ADC imaging of gene therapy

The flexibility of diffusion MRI in preclinical animal studies is evidenced by a recent study of two gene therapy regimens [29]. The use of a yeast cytosine deaminase transgene to convert the relatively innocuous 5-fluro-cytosine (5FC) to the cytotoxic 5-fluro-uracil (5FU) is one of the potential candidates for gene therapy of brain tumors. In this recent study two different transgenes for the conversion were constructed and evaluated for the therapeutic efficacy. The first (yCD transgene) relies on wild-type expression of UPRT to help convert 5FC to 5FU while the second (yCD-UPRT) has the UPRT protein fused to the yCD transgene. Figure 8 shows the results for three different 9L stable cell lines grown as orthotopic tumors: a wild-type 9L tumor, a tumor expressing the yCD transgene and another expressing the yCD-UPRT transgene. The animals with transgene tumors were treated with 1 g/kg of 5FC for ten consecutive days while the animals with wild-type 9L tumors were treated with vehicle only. Figures 8a, b and c show that the two therapies are clearly different. Both the animals containing transgene 9L tumors showed significant tumor regression and increased ADC. However, the increase in ADC within the yCD-UPRT tumors was markedly increased over the yCD tumor. These results were corroborated by those of a larger cohort of animals (Fig. 8d–f). It was found that, although tumor volume (Fig. 8d) showed no differences between the yCD and yCD-UPRT transgenes, the ADC changes were significantly higher in the yCD-UPRT tumors from days 7 through 15 (Fig. 8e). This higher ADC change corresponded to a much-improved animal survival rate of the yCD-UPRT therapy over yCD (Fig. 8f).

Diffusion heterogeneity

One final application of the use of ADC imaging as a surrogate marker of therapeutic efficacy that has yet to be investigated fully but was alluded to in a recent report [30] is the use ADC imaging to quantify heterogeneity of response. Figure 9 shows how diffusion is effective at identifying regions that show a poor response to therapy. In this case a rat bearing a 9L tumor had a highly effective

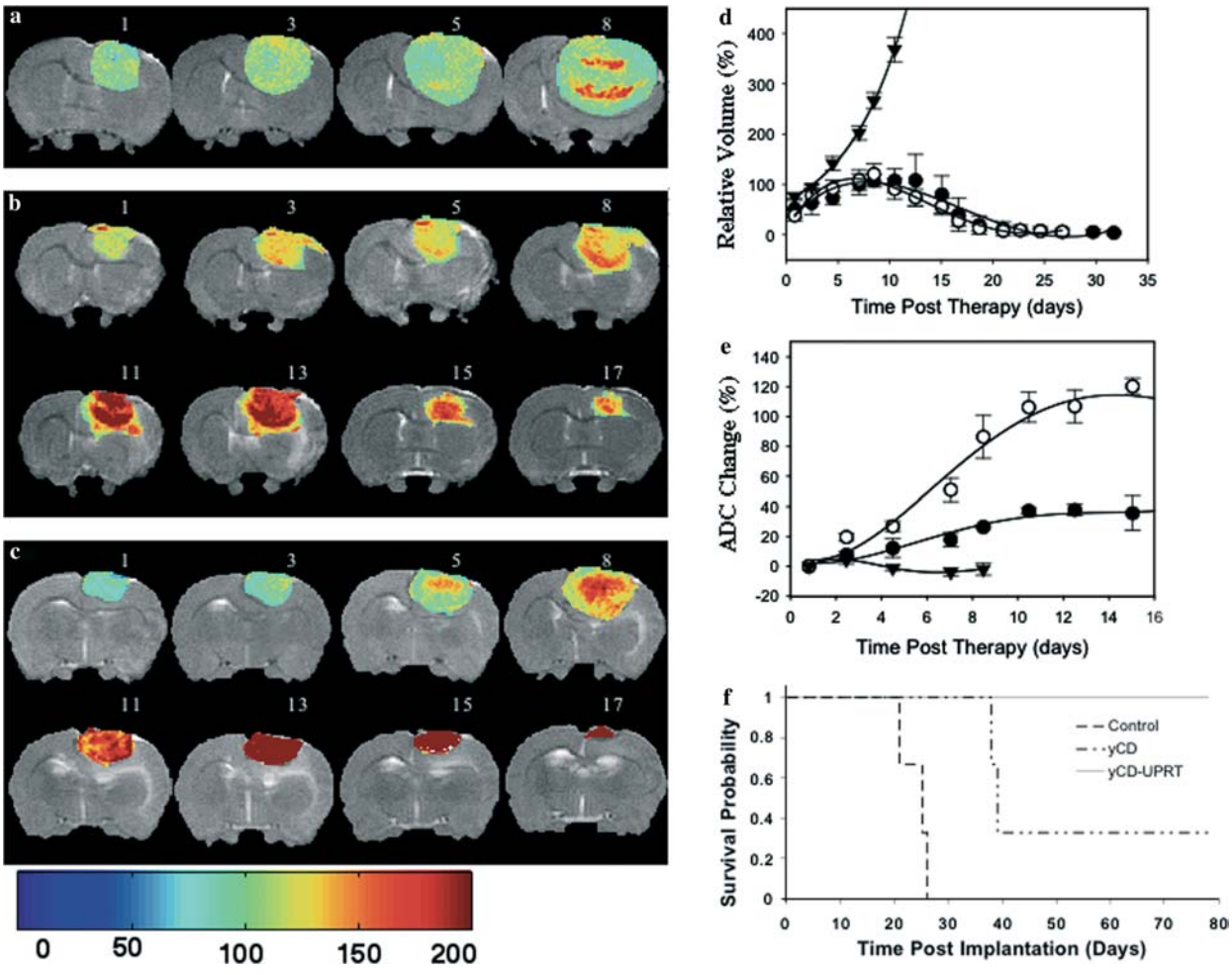

Fig. 8 Individual T2-weighted coronal MRI through the largest cross section of tumor acquired at the first day of treatment (day 1) and serially afterward. The map of apparent diffusion coefficients is overlaid in a color wash with blue representing low diffusion and red high diffusion. Wild-type 9L tumor (**a**) treated with PBS. CD expressing (**b**) or CD-UPRT expressing (**c**) treated with daily 5FC (1,000 mg/kg for 10 days). Tumor volume (**d**) and relative ADC values (**e**) as a function of time post treatment for wild-type 9L tumors treated with PBS (*closed triangles*) or for CD-expressing (closed circles) or CD-UPRT expressing (open circles) 9L tumors treated with 5FC (1,000 mg/kg i.p. daily for 10 days starting at day 1). Data represent the mean and standard error for wild-type ($n=6$), CD-expressing ($n=3$), and CD-UPRT expressing ($n=6$) tumors. Kaplan–Meier survival curve (**f**) for animals as a function of time since implantation for wild-type 9L tumors treated with PBS (single dashed line, $n=6$) or for CD-expressing (broken dashed line, $n=3$) or CD-UPRT expressing (solid line, $n=64$) 9L tumors treated with 5FC (1000 mg/kg i.p. daily for 10 days starting at day 17 post implantation). (Used with permission of Hamstra et al. [29])

dose of BCNU injected directly into the tumor (DTI-015, Direct Therapeutics Inc.). However, it is clear on the diffusion overlays (Fig. 9a) that there is a small region at the base of the tumor that does not increase in ADC nearly as much as the bulk of the tumor (Fig. 9b). Although the tumor shrinks considerably, tumor cells within this small tumor focus where shown by diffusion MRI to have not been effectively treated and in fact served as the seed for tumor regrowth.

Discussion

In this review we have shown evidence that diffusion MRI in animal models can provide important information not only in understanding how to translate diffusion as a surrogate marker into the clinic, but also to gain important information with regards to dose escalation in preclinical drug-discovery experiments. It has also been shown that diffusion MRI provides a robust surrogate that can be used to investigate gene therapy and chemotherapy regimens in both subcutaneous and orthotopic tumor models.

For preclinical drug studies using orthotopic animal tumor models, animal survival or animal morbidity are traditional therapeutic endpoints for quantification of treatment efficacy. The use of diffusion MRI offers a significant improvement over these traditional approaches

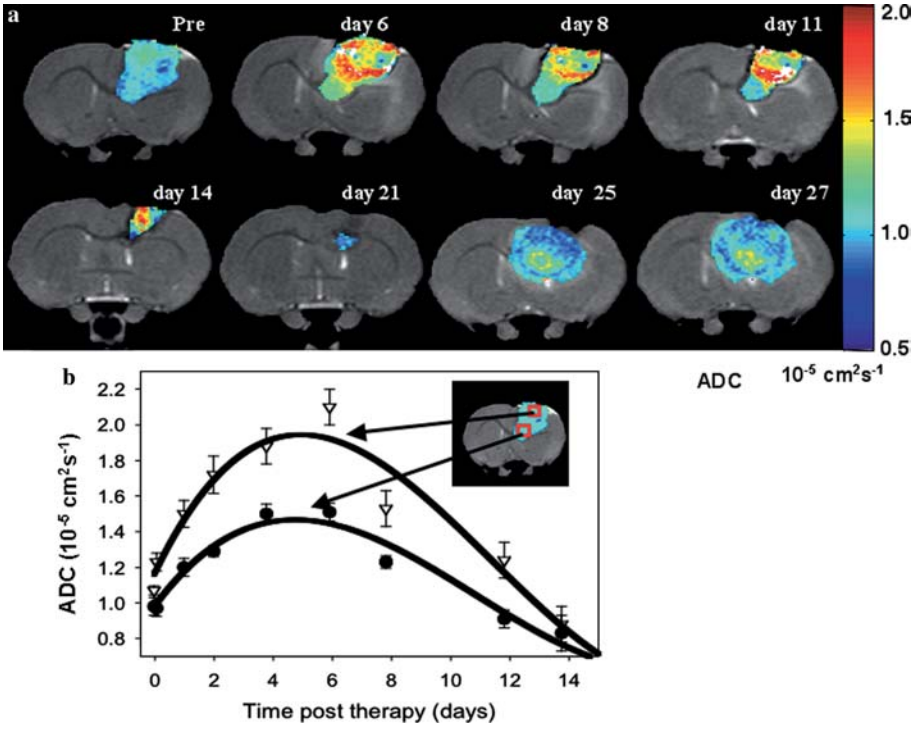

Fig. 9 Diffusion study of direct injection of BCNU (DTI-015, Direct Therapeutics, unpublished data). Panel A represents individual T2-weighted coronal MRI through the largest cross section of tumor for the animal treated with DTI-015 which subsequently was documented to have recurrence. Images were acquired prior to treatment (pre-) and serially afterward. The map of apparent diffusion coefficients is overlaid in a color wash with blue representing low diffusion (ADC = 0.5) and red high diffusion (ADC = 2.0). In Panel B the ADC values for the indicated regions of interest are plotted as a function of time in days since injection of DTI-015. The large central mass of tumor is indicated with *open circles*, and the small ventral medial lobe of tumor is indicated with *closed circles*. (Used with permission of Hall et al. [30])

including the ability to use the same animal as its own control, greater sensitivity to relatively small therapeutic effects, the ability to quantify effects of varying the drug dosage and timing, and finally, the potential of requiring smaller numbers of animals to obtain statistical significance. This latter issue can be especially important if variables such as heterogeneity of tumor take or growth rates are properties of the tumor model used. Another important aspect of the use of diffusion MRI is that it is translatable from the animal model into a clinical trial, which could thus provide a valuable quantitative and sensitive surrogate marker for therapeutic monitoring. Presently, a comparison of sequential MRI or computed tomography scans is the method of choice for monitoring the response of solid tumors to therapy, which compares the change in cross-sectional area of the tumor via the product of the maximal perpendicular tumor diameters or full volume determination [31,32]. For MRI, gadolinium-enhanced T1-weighted images are often used, but T2-weighted or other MR contrast strategies may be used. Comparisons of tumor burden are usually made between pretreatment scans and those obtained weeks to months after the conclusion of a therapeutic protocol [31,32]. Methods such as diffusion MRI for assessing treatment response that are not dependent on relatively slow changes in tumor volume may be capable of providing earlier indications of therapeutic outcome because molecular and cellular changes typically precede observable macroscopic changes in gross tumor size. Therefore, the use of a quantitative MRI surrogate marker scheme such as water diffusion for determination of therapeutic induced changes in tumor cellularity is an area of active research investigation [14,17,21,22,33].

In conclusion, the ability of ADC to become an accepted surrogate of therapeutic efficacy will depend not on its ability to correlate with therapeutic efficacy but on its ability to predict it. Therefore much effort is needed to investigate the predictability of ADC imaging. Imaging ADC changes in preclinical therapeutic investigations will be vital for understanding just how universal ADC can be in predicting anti-cancer therapeutic efficacy.

Acknowledgements This work was supported by the following research grants: NIH/NCI PO1CA85878, P50CA093990, and R24CA83099

References

1. Curt GA (1994) The use of animal models in cancer drug discovery and development. Stem Cells 12(1):23–29
2. Crafts D, Wilson CB (1977) Animal models of brain tumors. Natl Cancer Inst Monogr 46:11–17
3. Peterson DL, Sheridan PJ, Brown WE Jr (1995) Animal models for brain tumors: historical perspectives and future directions. J Neurosurg 80(5):865–876
4. Rosenblum ML, Knebel KD, Wheeler KT, Barker M, Wilson CB (1975) Development of an in vitro colony formation assay for the evaluation of in vivo chemotherapy of a rat brain tumor. In Vitro 11(5):264–273
5. Rosenblum ML, Knebel KD, Vasquez DA, Wilson CB (1976) In vivo clonogenic tumor cell kinetics following 1,3-bis(2-chloroethyl)-1-nitrosourea brain tumor therapy. Cancer Res 36(10):3718–3725
6. Barker M, Hoshino T, Gurcay O et al. (1973) Development of an animal brain tumor model and its response to therapy with 1,3-bis(2-chloroethyl)-1-nitrosourea. Cancer Res 33(5):976–986
7. Kim B, Chenevert TL, Ross BD (1995) Growth kinetics and treatment response of the intracerebral rat 9L brain tumor model: a quantitative in vivo study using magnetic resonance imaging. Clin Cancer Res 1(6):643–650
8. Ross BD, Chenevert TL, Kim B, Ben-Joseph O (1994) Magnetic resonance imaging and spectroscopy: application to experimental neuro-oncology. Q Magn Reson Biol Med 1:89–106
9. Ross BD, Chenevert TL, Rehemtulla A (2002) Magnetic resonance imaging in cancer research. Eur J Cancer 38(16):2147–2156
10. Ross BD, Moffat BA, Lawrence TS et al. (2003) Evaluation of cancer therapy using diffusion magnetic resonance imaging. Mol Cancer Ther 2(6):581–587
11. Stegman LD, Rehemtulla A, Hamstra DA et al. (2000) Diffusion MRI detects early events in the response of a glioma model to the yeast cytosine deaminase gene therapy strategy. Gene Ther 7(12):1005–1010
12. Zhao M, Pipe JG, Bonnett J, Evelhoch JL (1996) Early detection of treatment response by diffusion-weighted 1H-NMR spectroscopy in a murine tumour in vivo. Br J Cancer 73(1):61–64
13. Rehemtulla A, Hall DE, Stegman LD et al. (2002) Molecular imaging of gene expression and efficacy following adenoviral-mediated brain tumor gene therapy. Mol Imaging 1(1):43–55
14. Chenevert TL, Stegman LD, Taylor JM et al. (2000) Diffusion magnetic resonance imaging: an early surrogate marker of therapeutic efficacy in brain tumors. J Natl Cancer Inst 92(24):2029–2036
15. Chenevert TL, McKeever PE, Ross BD (1997) Monitoring early response of experimental brain tumors to therapy using diffusion magnetic resonance imaging. Clin Cancer Res 3(9):1457–1466
16. Brunberg JA, Chenevert TL, McKeever PE et al. (1995) In vivo MR determination of water diffusion coefficients and diffusion anisotropy: correlation with structural alteration in gliomas of the cerebral hemispheres. AJNR Am J Neuroradiol 16(2):361–371
17. Kauppinen RA (2002) Monitoring cytotoxic tumour treatment response by diffusion magnetic resonance imaging and proton spectroscopy. NMR Biomed 15(1):6–17
18. Hakumaki JM, Poptani H, Puumalainen AM et al. (1998) Quantitative 1H nuclear magnetic resonance diffusion spectroscopy of BT4C rat glioma during thymidine kinase-mediated gene therapy in vivo: identification of apoptotic response. Cancer Res 58(17):3791–3799
19. Galons JP, Altbach MI, Paine-Murrieta GD, Taylor CW, Gillies RJ (1999) Early increases in breast tumor xenograft water mobility in response to paclitaxel therapy detected by non-invasive diffusion magnetic resonance imaging. Neoplasia 1(2):113–117
20. Chenevert TL, Meyer CR, Moffat BA et al. (2002) Diffusion MRI: a new strategy for assessment of cancer therapeutic efficacy. Mol Imaging 1(4):336–343
21. Mardor Y, Pfeffer R, Spiegelmann R et al. (2003) Early detection of response to radiation therapy in patients with brain malignancies using conventional and high b-value diffusion-weighted magnetic resonance imaging. J Clin Oncol 21(6):1094–1100
22. Mardor Y, Roth Y, Lidar Z et al. (2001) Monitoring response to convection-enhanced taxol delivery in brain tumor patients using diffusion-weighted magnetic resonance imaging. Cancer Res 61(13):4971–4973
23. Mori S, van Zijl PC (1995) Diffusion weighting by the trace of the diffusion tensor within a single scan. Magn Reson Med 33(1):41–52
24. Wong EC, Cox RW, Song AW (1995) Optimized isotropic diffusion weighting. Magn Reson Med 34(2):139–143
25. Pipe JG, Chenevert TL (1991) A progressive gradient moment nulling design technique. Magn Reson Med 19(1):175–179
26. Anderson AW, Gore JC (1994) Analysis and correction of motion artifacts in diffusion weighted imaging. Magn Reson Med 32(3):379–387
27. Le Bihan D, Breton E, Lallemand D, Grenier P, Cabanis E, Laval-Jeantet M (1986) MR imaging of intravoxel incoherent motions: application to diffusion and perfusion in neurologic disorders. Radiology 161(2):401–407
28. Stejskal EO, Tanner J (1965) Spin diffusion measurements: spin-echoes in the presence of a time-dependent field gradient. J Chem Phys 42:288–292
29. Hamstra DA, Tychewicz JM, Lee KC et al. (2004) 19F Spectroscopy and diffusion weight MRI predict increased tumor response to cytosine deaminase and uracil phosphoribosyl transferase gene dependent enzyme prodrug therapy. Mol Ther 10(5): 916–928
30. Hall DE, Moffat BA, Stojanovska J et al. (2004) Therapeutic Efficacy of DTI-015 using diffusion MRI as an Early Surrogate Marker. Clin Cancer Res 10(23): 7852–7859
31. James K, Eisenhauer E, Christian M et al. (1999) Measuring response in solid tumors: unidimensional versus bidimensional measurement. J Natl Cancer Inst 91(6):523–528
32. Macdonald DR, Cascino TL, Schold SC Jr, Cairncross JG (1990) Response criteria for phase II studies of supratentorial malignant glioma. J Clin Oncol 8(7):1277–1280
33. Ross BD, Chenevert TL, Garwood M et al. (2003) Evaluation of (*E*)-2'-deoxy-2'-(fluoromethylene)cytidine on the 9L rat brain tumor model using MRI. NMR Biomed 16(2):67–76